THE JOURNAL OF BIOLOGICAL CHEMISTRY VOL. 286, NO. 35, pp. 30600–30605, September 2, 2011

Probing Protonation/Deprotonation of Tyrosine Residues in Cytochrome ba_3 Oxidase from *Thermus thermophilus* by Time-resolved Step-scan Fourier Transform Infrared Spectroscopy*

Received for publication, April 18, 2011, and in revised form, July 5, 2011 Published, JBC Papers in Press, July 12, 2011, DOI 10.1074/jbc.M111.252213

Constantinos Koutsoupakis[‡], Olga Kolaj-Robin[§], Tewfik Soulimane[§], and Constantinos Varotsis[‡1]

From the [‡]Department of Environmental Science and Technology, Cyprus University of Technology, 3603 Lemesos, Cyprus and the [§]Chemical and Environmental Science Department and Materials & Surface Science Institute, University of Limerick, Limerick, Ireland

Elucidating the properties of the heme Fe-Cu_B binuclear center and the dynamics of the protein response in cytochrome *c* oxidase is crucial to understanding not only the dioxygen activation and bond cleavage by the enzyme but also the events related to the release of the produced water molecules. The time-resolved step-scan FTIR difference spectra show the ν_{7a}(CO) of the protonated form of Tyr residues at 1247 cm^{-1} and that of the deprotonated form at 1301 cm^{-1}. By monitoring the intensity changes of the 1247 and 1301 cm^{-1} modes as a function of pH, we measured a pK_a of 7.8 for the observed tyrosine. The FTIR spectral changes associated with the tyrosine do not belong to Tyr-237 but are attributed to the highly conserved in heme-copper oxidases Tyr-136 and/or Tyr-133 residue (Koutsoupakis, K., Stavrakis, S., Pinakoulaki, E., Soulimane, T., and Varotsis, C. (2002) *J. Biol. Chem.* 277, 32860–32866). The oxygenation of CO by the mixed-valence form of the enzyme revealed the formation of the ~607 nm P (Fe(IV)=O) species in the pH 6–9 range and the return to the oxidized form without the formation of the 580 nm F form. The data indicate that Tyr-237 is not involved in the proton transfer pathway in the oxygenation of CO by the mixed-valence form of the enzyme. The implication of these results with respect to the role of Tyr-136 and Tyr-133 in proton transfer/gating along with heme a_3 ring D propionate-H_2O-ring A propionate-Asp-372 site to the exit/output proton channel (H_2O pool) is discussed.

Cytochrome ba_3 oxidase is a member of the heme-copper oxidase family and, in addition to activating O_2 and conserving the energy of O_2 reduction for subsequent ATP synthesis, is able to catalyze the reduction of NO to N_2O under reducing anaerobic conditions (1–5). The crystal structure of the protein indicates that subunit I consists of a low-spin heme b and a high-spin heme a_3-Cu_B binuclear center where the dioxygen and nitric oxide reactions take place (1). Two proton pathways have been identified in ba_3 oxidase and correspond to the putative so-called K and D pathways found in *Paracoccus denitrificans* and bovine oxidase despite the fact that most of the residues belonging to these pathways are not conserved (1). Glu-278 (residue of *P. denitrificans*), which is highly conserved in heme-copper oxidases and is involved in redox-induced proton transfer reactions, is replaced by Ile in ba_3 oxidase (1, 6, 7). The highly conserved, covalently ring-linked His-Tyr species that has been determined by the crystal structures of bovine, *P. denitrificans*, and *Thermus thermophilus* heme-copper oxidases and by protein chemical analysis is a unique peptide (1, 6, 7). It is located in the immediate vicinity of the binuclear center, within hydrogen-bonding distance of heme a_3-ligated O_2, and is capable of modulating the redox potential and the pK_a of Tyr-O-His as occurs for the redox-active, covalently cross-linked tyrosine residue in galactose oxidase (8). On the basis of the crystal structure of the bovine enzyme, Yoshikawa *et al.* (6) proposed a proton transfer mechanism from this tyrosine to ferric peroxide to generate a hydroperoxo adduct. Recently, the reaction of ba_3 oxidase with O_2 was investigated by time-resolved optical spectroscopy, and the results indicated the formation of oxygenated intermediate species (9). The molecular mechanisms of the ba_3 oxidase are expected to be similar to those of other distantly related heme-copper oxidases with respect to the oxygen chemistry and the oxygenation of CO to form the 607 nm P intermediate ferryl-oxo species (6–11). The latter reaction was first reported in the oxygen-dependent oxidation of carbon monoxide in mammalian tissue (12). Mammalian cytochrome *c* oxidase was demonstrated to catalyze the monooxygenation of CO to CO_2 when reductively activated in the presence of oxygen (13).

In the O_2 cycle of oxidases, it has been suggested that the O–O bond cleavage proceeds by concerted hydrogen atom transfer from the cross-linked His-Tyr species to produce the Fe(IV)=O/Cu(II)$_B$-H-Y· species (14). This raises important issues as to the means by which the electron transfer to these transient species is regulated for conformational transitions that are required for any pumping mechanism to occur (6, 7, 9, 10). In the oxidase/peroxide reaction at high pH, it has been demonstrated that the addition of stoichiometric amounts of H_2O_2 to oxidized enzyme leads to the formation of the 607 nm form having the proposed Fe(IV)=O . . . HO-Cu(II)$_B$-His-Tyr· structure (15). Furthermore, single protonation of the former species results in the formation of the 580 nm form with a

* This work was supported by research funds from the Cyprus University of Technology (to C. V.) and the Science Foundation Ireland Grant BICF865 (to T. S.).

[1] To whom correspondence should be addressed. Tel.: 357-2500-2451; Fax: 357-2500-2802; E-mail: c.varotsis@cut.ac.cy.

proposed Fe(IV)=O $Cu(II)_B$-His-Tyr$^{\bullet}$ structure (15). However, no definite spectroscopic evidence has yet been observed for the formation of Tyr$^{\bullet}$ in the binuclear center of heme-copper oxidases. It has been suggested that the additional electron needed to produce the 607 nm P (Fe(IV)=O) species is provided by Tyr-167 or Trp-272 (*P. denitrificans* sequence), which are near the binuclear heme Fe-Cu_B center and highly conserved in heme-copper oxidases (Tyr-136 and Trp-229 in *T. thermophilus*) (16, 17). Determining the properties of the residue(s) responsible for the formation of the 607 nm P (Fe(IV)=O) species will resolve controversial aspects of the oxygen activation and O–O cleavage mechanisms.

FTIR spectroscopy has proven to be a very powerful technique in studying changes at the level of individual amino acids during protein action (18, 19). FTIR studies of a His-Tyr-OH model compound, 2-imidazol-1-yl-4-methylphenol, have demonstrated that the ν_{7a}(CO) and δ(COH) modes in the deprotonated form of His-Tyr-O^- shift from 1268 cm^{-1} (protonated) to 1301 cm^{-1} (18). In addition, the oxidized-minus-reduced FTIR spectra of aa_3 oxidase from *P. denitrificans* showed signals at 1270 cm^{-1} that were attributed to ν_{7a}(CO) and δ(COH) of a protonated tyrosine (18). The observed reduced intensity of these signals in the Y280H mutant allowed Hellwig *et al.* (18) to assign this mode to ν_{7a}(CO) and δ(COH) of the protonated cross-linked Tyr-237 residue (Tyr-280 in *P. denitrificans*). With the purpose of identifying His-Tyr-OH modes in cytochrome bo_3 oxidase, Woodruff and co-workers (19) applied low-temperature FTIR difference spectroscopy to the enzyme and FTIR spectroscopy to the His-Tyr-OH model compound. They detected the fundamental His N_ϵ-C_ϵ Tyr mode and its combination at 1549 and 3033 cm^{-1}, respectively (19).

In addition to the dioxygen activation and reduction and the oxygenation of CO mechanisms, it is crucial to determine the intermediate protein structures subsequent to ligand binding/release and discrimination (20). Extensive time-resolved step-scan FTIR (TRS^2-FTIR)[2] studies of ba_3 oxidase-CO have revealed the dynamics of the binuclear center and showed protein conformational changes near the heme a_3 propionates (4, 5, 21, 22). In addition, the ligand delivery channel at the Cu_B site and the presence of a docking site near the heme a_3 propionates were identified (21, 22). Cytochrome ba_3 has preexisting cavities that are only modestly perturbed by the photodissociated CO from heme a_3, and previous work revealed such a docking site that is responsible for the kinetic control of both ligand motion/binding and escape (21). Those results, in conjunction with the reported protonic connectivity between the propionates of heme a_3, Asp-372, and H_2O, led to the identification of a proton exit channel (22). A pathway connecting the docking and binding sites was presented to explain how this pathway may lead to the escape of translocated protons and catalytically formed H_2O molecules. Of note, both protonated and deprotonated forms of the ring A of heme a_3 were detected in the TRS^2-FTIR data (22).

The identification of ionizable groups whose pK_a values are near physiological pH is extremely useful because the conformational transition that is associated with such protonation/deprotonation events is crucial in our understanding of the proton motion in heme-copper oxidases. TRS^2-FTIR spectroscopy has been applied to the carbonmonoxy derivatives of heme-copper oxidases to probe the protein dynamics subsequent to CO photolysis (22). The TRS^2-FTIR spectra are the result of the perturbation induced by the photodissociation of CO from the heme iron and its subsequent binding to Cu_B to structures near heme iron and Cu_B. In the work presented here, we continued our TRS^2-FTIR approach with heme-copper oxidases at room temperature, and in conjunction with the assignment of ν_{7a}(CO) and δ(COH) in the aa_3-type oxidase from *P. denitrificans*, we detected the protonated and deprotonated forms of tyrosine residue(s) near the induced perturbation, *i.e.* the heme a_3-Cu_B binuclear center of cytochrome ba_3 from *T. thermophilus* (4, 5, 17, 18, 23, 24). Our TRS^2-FTIR difference spectra show that ν_{7a}(CO) and δ(COH) in the protonated form of Tyr are located at 1247 cm^{-1} and in the deprotonated form at 1301 cm^{-1}. By monitoring the intensity changes of the 1247 and 1301 cm^{-1} modes as a function of pH, we measured a pK_a of 7.8 for the observed Tyr residue. On the basis of the tentative assignments of the 1247 and 1301 cm^{-1} modes, the data indicate that Tyr-133 and/or Tyr-136 (both of which are located near the binuclear center) serves as a proton gating/transfer ionizable group. Mixed-valence ba_3 oxidase is a two-electron reduced form of the enzyme (heme a_3^{2+}-Cu_B^{1+}) that carries out O_2 reduction only to the controversial peroxy oxidation level. Upon direct mixing of O_2 with the mixed-valence CO-bound enzyme (MV-CO) under alkaline and acidic conditions, the ~607 nm P (Fe(IV)=O) species is formed. This intermediate is linked to the proton pump function of heme-copper oxidases (6, 7, 15). Our data obtained under both acidic and alkaline conditions do not favor the cross-linked Tyr-237 residue (whose protonation state is not altered between pH/pD 5.5 and 9.7), as the residue associated with the FTIR spectral changes, but other tyrosine residues with labile protons. We postulate that Tyr-133 and/or Tyr-136 (both of which are the only Tyr residues with labile protons near the vicinity of the heme Fe-Cu_B binuclear center) plays a role in either the dioxygen chemistry or proton gating during the enzymatic reactions.

EXPERIMENTAL PROCEDURES

Cytochrome ba_3 was isolated from *T. thermophilus* HB8 cells according to previously published procedures (2). The samples used for the FTIR measurements had an enzyme concentration of ~1 mM and were placed in the desired buffer (pH 5.5–6.5, MES; pH 7.5, HEPES; or pH 8.5–9.5, CHES). Dithionite-reduced samples were exposed to 1 atm CO (1 mM) in an anaerobic cell to prepare the carbonmonoxy adduct and transferred to a tightly sealed FTIR cell under anaerobic conditions (l = 15 μm). CO gas was obtained from Messer. The 532-nm pulse from a Continuum Nd:YAG laser (7-ns width, 3 Hz) was used as a pump light (4 mJ/pulse) to photolyze the ba_3-CO oxidase. FTIR measurements were performed on a Bruker Equinox IFS 55 spectrometer equipped with the step-scan option. For the time-resolved experiments, a TTL (transistor-transistor logic)

[2] The abbreviations used are: TRS^2-FTIR, time-resolved step-scan FTIR; MV-CO, mixed-valence CO-bound; CHES, 2-(cyclohexylamino)ethanesulfonic acid.

pulse provided by a digital delay pulse generator (Quantum Composers 9314T) triggers, in order, the flashlamps, Q-switch, and FTIR spectrometer. Pretriggering the FTIR spectrometer to begin data collection before the laser fires allows 11 fixed reference points to be collected at each mirror position, which are used as the reference spectrum in the calculation of the difference spectra. Changes in intensity were recorded with an MCT (mercury-cadmium-telluride) detector (Graseby Infra-Red D316, response limit of 600 cm^{-1}) amplified in the DC-coupled mode and digitized with a 200-kHz 16-bit analog-to-digital converter. A broadband interference optical filter (Optical Coating Laboratory, Santa Rosa, CA) with a short wavelength cutoff at 2.67 μm was used to limit the free spectral range from 2.67 to 8 μm. This leads to a spectral range of 3949.5 cm^{-1}, which is equal to an undersampling ratio of 4. Single-sided spectra were collected at 8 cm^{-1} spectral resolution, 5-μs time resolution, and 10 co-additions per data point. The total accumulation time for each measurement was 62 min, and two to three measurements were collected and averaged. A Blackman-Harris three-term apodization function with 32 cm^{-1} phase resolution and the Mertz phase correction algorithm were used. Difference spectra were calculated by substracting the reference spectrum, recorded before the laser firing, from those after the photodissociation of CO from heme a_3.

The MV-CO enzyme was prepared by exposing an anaerobic solution of the resting enzyme to CO for 10 h at 20 °C. The 610 nm species was obtained by introducing O_2 to the MV-CO enzyme. Optical absorption spectra were recorded with a Perkin-Elmer Lambda UV-visible spectrometer before and after the FTIR measurements to ensure the formation and stability of the CO adducts.

RESULTS AND DISCUSSION

pK_a of the Tyrosine Residue—Intensity changes and frequency shifts of side chains and backbone structures have been observed in the FTIR difference spectra of heme-copper oxidases as the result of an electrochemical perturbation (oxidized minus reduced) of the metal centers at room temperature or of the perturbation induced by the photodissociation of CO bound to the heme at 80 K, at which the CO binds irreversibly to Cu_B (18, 19, 23, 24). In the latter case, the perturbation induced by the photodissociated CO exerts its main effect on the environment of the binuclear center. The kinetics data on the photodissociation of CO and its rebinding to heme a_3 have shown that the CO ligation/release mechanism in cytochrome ba_3 follows that found in other heme-copper oxidases and proceeds according to Scheme 1.

$$Fe^{2+},Cu_B^{+} + CO \underset{k_{-1}}{\overset{k_1}{\rightleftharpoons}} \underset{A}{Fe^{2+},Cu_B^{+}\text{-}CO} \underset{k_{-2}}{\overset{k_2}{\rightleftharpoons}} \underset{B}{Fe^{2+}\text{-}CO,Cu_B^{+}}$$

SCHEME 1

In contrast to the bovine aa_3 oxidase, Cu_B of cytochrome ba_3 has a relatively high affinity for CO ($K_1 > 10^4$), whereas the transfer of CO to heme $a_3{}^{2+}$ is characterized by a small $k_2 = 8$ s^{-1} and by $k_{-2} = 0.8$ s^{-1}, which is 30-fold greater than that of

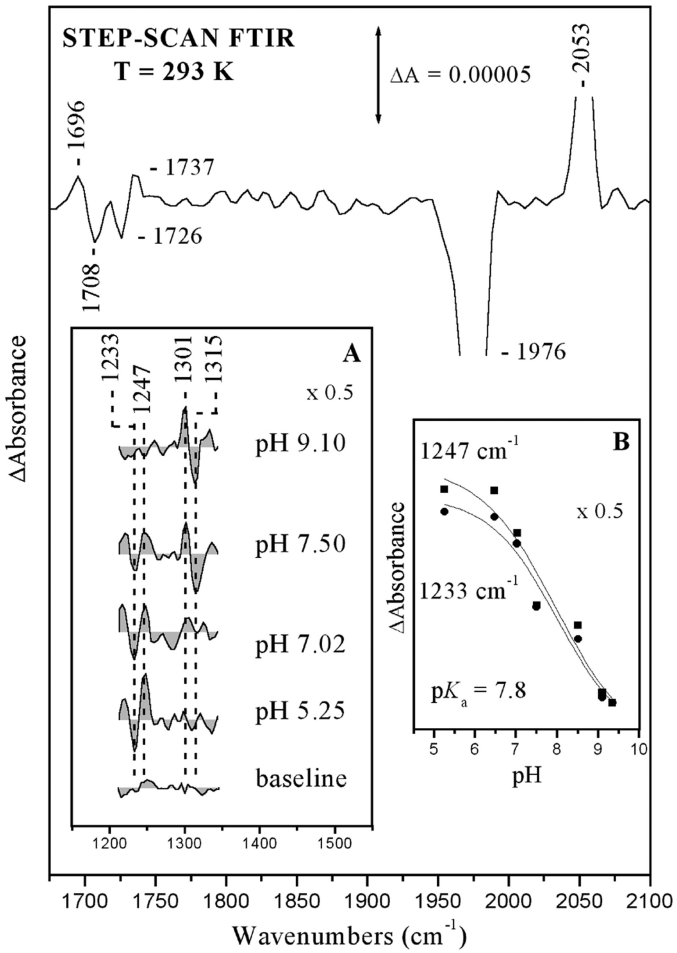

FIGURE 1. **TRS^2-FTIR difference spectrum (1675–2100 cm^{-1} spectral region) of the CO-bound form of fully reduced cytochrome ba_3 oxidase at pH 7.5 and 293 K.** The spectrum is the average of 40 individual spectra from 0 to 200 μs. The spectral resolution was 8 cm^{-1}, the time resolution was 5 μs, and 10 co-additions were collected per data point. The photolysis wavelength was 532 nm (4 mJ/pulse), and three measurements were recorded and averaged. *Inset A*, TRS^2-FTIR difference spectra (1200–1350 cm^{-1} spectral region) of the ba_3 oxidase-CO complex subsequent to CO photolysis at the indicated pH values. The experimental conditions were the same as described above. *Inset B*, plot of the 1247 cm^{-1} (■) and 1233 cm^{-1} (●) modes *versus* pH. ΔA values of the 1233 and 1247 cm^{-1} modes were measured from the peaks area, and the curves are three-parameter sigmoidal fits to the experimental data.

bovine aa_3 oxidase (25). Therefore, it is possible to take advantage of the long life-time of the $Cu_B{}^{1+}$-CO complex and collect TRS^2-FTIR difference spectra at room temperature, in which maximum conformational changes and possible proton transfer reactions can take place. It should be noted that small conformational changes of the protein are expected at low temperatures, and thus, it is unlikely that proton transfer reactions can take place. In our room temperature TRS^2-FTIR difference spectra, the positive bands are associated with the $Cu_B{}^{1+}$-CO state, and the negative bands are due the heme a_3 Fe^{2+}-CO state.

Fig. 1 shows the TRS^2-FTIR difference spectrum (the co-averaged first 200 μs after photodissociation of CO) at pH 7.5. In this time scale, the photodissociated CO from the heme a_3 iron (ν(CO) = 1976 cm^{-1}) is bound to Cu_B (ν(CO) = 2053 cm^{-1}). The data show that photodissociation of CO from heme a_3 produces the same transient photoproduct as that obtained at pD

8.5 and without changes in the intensity ratio of the 1976/2053 cm^{-1} modes (4, 5). In addition, the C=O mode of the protonated heme a_3 propionates is seen as a derivative shape feature with a trough/peak at 1708/1696 cm^{-1}; the negative band located at 1726 cm^{-1} is the C=O stretch of Asp-372. ν_{7a}(CO) and δ(COH) of the protonated and deprotonated forms of tyrosine residues are expected in the 1200–1300 cm^{-1} region (18). A close inspection of the data indicates that such features exist in the TRS^2-FTIR difference spectrum (t_d = 0–200 μs) at pH 7.5 and appear as two pairs of peaks/troughs at 1247/1233 and 1301/1315 cm^{-1}. The pH dependence of both pairs of the peaks/troughs is depicted in Fig. 1 (*inset A*). The TRS^2-FTIR difference spectrum obtained at pH 9.1 indicates that the 1233/1247 cm^{-1} pair observed in the pH 5.5–7.5 range has vanished and that the 1301/1315 cm^{-1} pair has gained intensity relative to that observed at pH 7.5. On the basis of the similarity in the frequencies of the ν_{7a}(CO) and δ(COH) modes in the model compound and in the aa_3 oxidase from *P. denitrificans*, we assign the 1247 and 1301 cm^{-1} vibrations to the protonated and deprotonated forms of a tyrosine residue, respectively (18). The relative intensities (peak area) of the peak/trough pair at 1247/1233 cm^{-1} are shown in Fig. 1 (*inset B*) as a function of pH. An apparent pK_a of 7.8 was calculated from the titration curve. The pK_a value we have measured is in excellent agreement with that predicted at 7.6 from calculations but lower than that reported at 8.6 and 9.2 for the model compound 2-imidazol-1-yl-4-methylphenol (26–28). The model compound studies have also demonstrated that the linked imidazole group causes lowering of the pK_a of the phenolic OH by 1.5 pK_a units compared with that of the isolated *p*-cresol OH value (10.2). Although these studies did not include the influence of Cu_B on the phenol pK_a, the observed lowering of pK_a to 7.8 in the protein can be explained in terms of electron-withdrawing effects from Cu_B and therefore does not rule out the cross-linked Tyr-237 as being the residue responsible for the observed spectral changes (see below). The latter effect will be minimized due to d_π-p_π back-bonding and the weak coordination ability expected for His-233. The observed shift of the pK_a value from 8.6 to 9.2 in the model to 7.8 in the enzyme indicates a rather extended delocalization/stabilization of the Tyr anion involving either the Tyr-His-Cu_B structure or another group able to accept the negative charge. In the best scenario, this group could be the heme a_3 and not just Tyr-His or a similar dipeptide (29).

Protonation/Deprotonation State of Tyr Residues—In an attempt to determine which tyrosine is responsible for the spectral changes shown in Fig. 1, we examined the available crystal structure of cytochrome ba_3 (Protein Data Bank code 1EHK) (1). Subunit I contains 24 tyrosine residues, six of which are in a distance of <7 Å from the active center, whereas subunit II contains eight tyrosine residues and subunit IIa contains one, none of which are in close proximity to the heme Fe-Cu_B center. Fig. 3 shows the five tyrosine residues closest to the binuclear center of ba_3 oxidase, which appear to be the most possible candidates for the transient protonation/deprotonation events described above.

Tyr-237 is cross-linked to His-233, one of the Cu_B ligands, and is the closest tyrosine residue to the heme a_3 iron atom (5.63 Å). However, we do not favor Tyr-237 as the most possible candidate because its transient protonation/deprotonation would have a clear effect on the frequency of the transient Cu_B^{1+}-CO complex (4). The frequency of the transient Cu_B^{1+}-CO mode is at 2053 cm^{-1}, the same as in the equilibrium complex, and remained unchanged in the pH/pD 5.5–9.7 range. It has been clearly demonstrated that a change in the protonation state of one of the Cu_B imidazole ligands has a significant effect on the back-donation of electron density and therefore the vibrational frequencies with a calculated shift of 20–43 cm^{-1}, whereas deprotonation of the phenol unit strengthens the Cu–C bond and weakens the C–O bond, leading to a frequency shift of 11 cm^{-1} (30). On the basis of the experimental and theoretical studies, we concluded that the protonation state of Tyr-237 remains unchanged. Tyr-244 is ~7 Å from the heme OH group and Cu_B ligand His-283, respectively. Although Tyr-244 has been proposed to participate in one of the proton translocation channels, its position relative to the binuclear center does not support its involvement in the protonation/deprotonation events because, as shown in previous work, the effect of the CO photolysis is focused mainly in the region between heme a_3 iron, Cu_B, and heme propionates (4). Of the three remaining tyrosine residues, Tyr-373 is almost 7 Å from the COO group of Asp-372, a residue shown to be in hydrogen-bonding distance with the ring A heme a_3 propionate. Although the heme propionate-Asp-372 moiety is strongly involved in the CO photolysis event, the relatively long distance of Tyr-373 from the heme propionate (~10 Å) minimizes its possibility as a candidate for the observed changes we observed (4).

The last two tyrosine residues near the binuclear center are Tyr-133, whose hydroxyl oxygen atom is 2.67 Å from the ring D heme a_3 propionate, and Tyr-136, which is hydrogen-bonded to Trp-229 and proposed to be involved in a direct Cu_A-to-Cu_B electron transfer process (1). Trp-229 and Tyr-136 are near Cu_B and have been proposed to be involved in the formation of the 607 nm P (Fe(IV)=O) species in *P. denitrificans* (16, 17). For Tyr-133, the distance between the hydroxyl oxygen atom and the ring D heme a_3 propionate means that Tyr-133 and the COO propionate group are strongly hydrogen-bonded, and also, this tyrosine residue appears in a site proved to play significant role in the events after CO photolysis (4, 21, 22). In previous work, we showed that CO photolysis triggers conformational changes in the ring A heme a_3 propionate-Asp-372 moiety, which is also strongly hydrogen-bonded (21). We also showed that, upon dissociation, the photolyzed CO becomes trapped within a ligand-docking site located in the same region above heme a_3 (21). In this work, we present evidence for transient deprotonation of tyrosine residue(s), and we propose that Tyr-133, which is in hydrogen-bonding distance with the ring D heme a_3 propionate, forms an analogous bond with the ring A heme a_3 propionate-Asp-372 moiety and/or Tyr-136, which is near the Cu_B unit. These two tyrosine residues are likely to be subjected to the same conformational changes after CO photolysis and may serve as the entry/exit gate for the translocated protons during the catalytic function of the enzyme.

Formation of the 607 nm Ferryl-oxo Species—The ~607 nm (Fe(IV)=O) species that is formed after the decay of the oxy

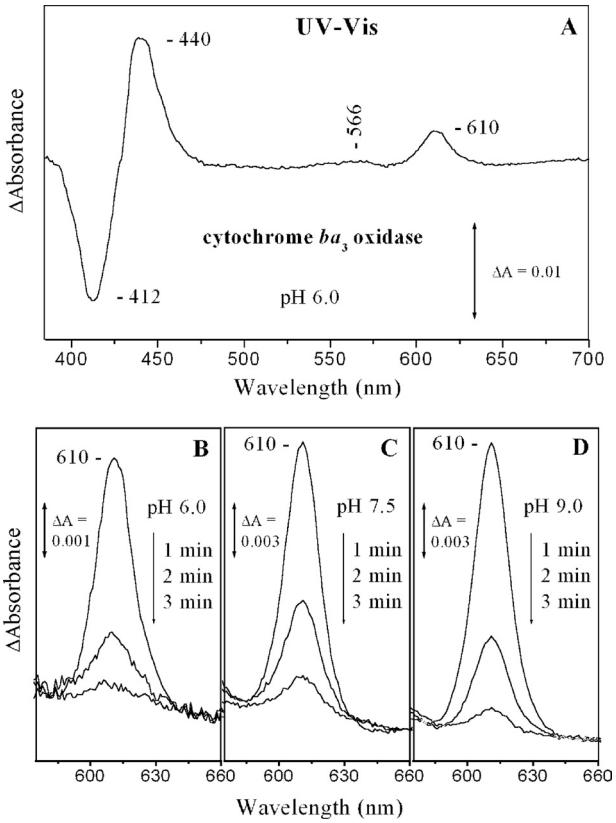

FIGURE 2. **Optical absorption difference spectra of the CO-MV cytochrome ba_3/O_2 reaction minus the resting form of the enzyme at 1, 2, and 3 min subsequent to mixing at pH 6.0 (*A* and *B*), pH 7.5 (*C*), and pH 9.0 (*D*).** The concentration of the enzyme was 10 μM, and the path length of the cell was 1 cm.

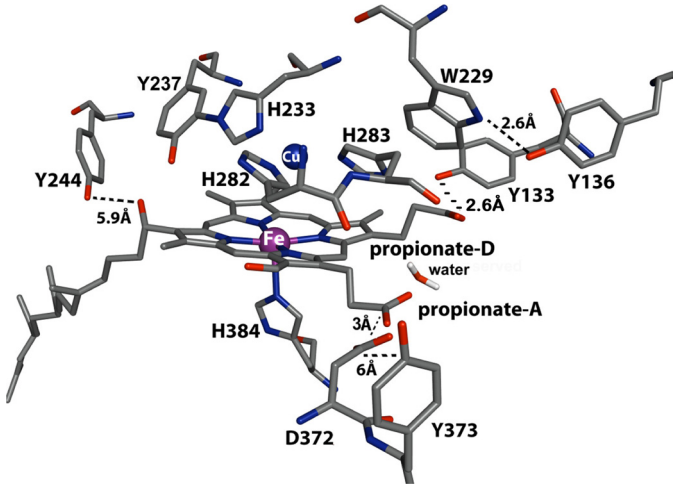

FIGURE 3. **Representation of the binuclear center of cytochrome ba_3 oxidase from *T. thermophilus* (Protein Data Bank code 1EHK).** The five tyrosine residues nearest the heme a_3-Cu_B center are also included. The figure was prepared with PyMOL (36).

intermediate in the MV/O_2 reaction may be generated either by direct mixing of O_2 with the MV-CO oxidase or by aerobic incubation of the enzyme with CO and O_2 (11, 31–35). Both approaches produce the ~607 nm species (P). We have applied the former procedure to both the wild-type and MV-Y280H aa_3 oxidases from *P. denitrificans* and demonstrated that the ~607 nm species can be formed in both the wild-type and Y280H enzymes (32). When O_2 was introduced to the MV-CO ba_3 enzyme at pH 6.0, the absorption difference spectrum (MV-CO/O_2 minus oxidized) shown in Fig. 2*A* was obtained. The maxima observed at 440, 566, and 610 nm and the minimum at 412 nm are in agreement with those reported previously for aa_3-type oxidases (31–33). Fig. 2 (*B–D*) shows the pH and time dependence of the 610 nm form at pH 6.0, 7.5, and 9. The 610 nm species was more populated above pH 7.5 (Fig. 2, *C* and *D*) and decayed faster as the pH was lowered (Fig. 2*B*). It should be noted that the formation of the 610 nm species persisted up to pH 12 (data not shown). The data indicate that O_2 spontaneously replaces CO, and the decay of the 610 nm species to the pulsed and subsequently to the resting form occurs on a time scale of tens of seconds, in agreement with previous results on the aa_3-type heme-copper oxidases (32, 33). For the sake of comparison with earlier work, in the following discussion, we ascribe the 610 nm species we detected in the MV/O_2 cytochrome ba_3 reaction to the species referred to in the literature as having 607 nm absorbance.

It has been proposed that the formation of the 607 nm species (P) is accompanied by the generation of a Cu_B-His-Tyr$^\bullet$ species, which is the result of a concerted hydrogen atom abstraction from Tyr by the iron-bound oxygen atom to promote O–O bond cleavage and formation of the P ferryl-oxo (Fe(IV)=O) species with a characteristic frequency at 804 cm^{-1} (14). Most recently, the 607 nm and 804 cm^{-1} ferryl-oxo species were detected at alkaline conditions (11). Tryptophan and tyrosine radicals have been also observed in the aa_3/H_2O_2 reaction forming the 607 nm species, and an analogous species has been observed in both the Y280H/H_2O_2 and MV-Y280H-CO/O_2 reactions (16, 17, 34). The data presented in Figs. 2 and 3 demonstrate that the 607 nm species (P) persists under alkaline conditions in the oxygenation reaction of the ba_3 oxidase-CO complex, in which the observed tyrosine(s) are deprotonated. If the pK_a of Tyr-237 is modulated by the ligand binding to heme a_3 (CO *versus* O_2), then we cannot exclude the possibility that Tyr-237 is the source of the third electron to produce the 607 nm species.

Combining the above results with the earlier optical and time-resolved resonance Raman results and with those reported recently on the formation of the 607 nm species in the MV/O_2 reaction (11, 31–35), the following points emerge. It has been conclusively demonstrated by this work that the incubation of oxidized ba_3 with CO forms the MV species, which reacts with O_2 to generate the P intermediate appearing in the physiological reaction of all heme-copper oxidase, but it does not yield the F intermediate (580 nm species). The rate of decay of the 607 nm species is faster under acidic conditions, indicating that, when Tyr-136/Tyr-133 is protonated, the ferryl-oxo species decays faster to the pulsed and subsequently to the resting form of the enzyme. Under alkaline conditions, Tyr-136/Tyr-133 is deprotonated, and O_2 binding to heme a_3 is followed by oxidation of an amino acid residue. In the latter case, the O–O scission occurs by electron transfer, forming only one highly oxidizing species (607 nm species). The slow rate of decay of the 607 nm species under alkaline conditions indicates that the protonation state of Tyr-136/Tyr-133 is coupled to its

decay to the pulsed/oxidized form. We propose that uptake of a proton from the bulk solution is accompanied by the protonation of Tyr-136 and/or Tyr-133. In this way, protons are transferred to the ring D propionate-H_2O-ring A propionate-Asp-372 site. All residues involved in the proposed proton transfer mechanism are highly conserved among the structurally known heme-copper oxidases and form functionally operating residues that are part of an exit/output proton channel. The sequential or concerted hydrogen-bonded connectivity between the operating residues has an activation for proton motion. The exchangeable protons play a vital role in the biological function of the enzyme, and the first step in locating protein (in this case, tyrosine(s)) residues near the binuclear center as possible sites for proton motion has been demonstrated in this work. The data presented here, coupled with those reported recently by Chang *et al.* (37), who demonstrated that ba_3 oxidase utilizes only one proton input channel analogous to the A-family K-channel, support the idea that a common active structure is responsible for the function of cytochrome oxidase. The labile protons could be either redox-linked or perturbed by ligand motion, including H_2O molecules. Experiments are in progress to answer these questions.

REFERENCES

1. Soulimane, T., Buse, G., Bourenkov, G. P., Bartunik, H. D., Huber, R., and Than, M. E. (2000) *EMBO J.* **19,** 1766–1776
2. Buse, G., Soulimane, T., Dewor, M., Meyer, H. E., and Blüggel, M. (1999) *Protein Sci.* **8,** 985–990
3. Giuffrè, A., Stubauer, G., Sarti, P., Brunori, M., Zumft, W. G., Buse, G., and Soulimane, T. (1999) *Proc. Natl. Acad. Sci. U.S.A.* **96,** 14718–14723
4. Koutsoupakis, K., Stavrakis, S., Pinakoulaki, E., Soulimane, T., and Varotsis, C. (2002) *J. Biol. Chem.* **277,** 32860–32866
5. Koutsoupakis, K., Stavrakis, S., Soulimane, T., and Varotsis, C. (2003) *J. Biol. Chem.* **278,** 14893–14896
6. Yoshikawa, S., Shinzawa-Itoh, K., Nakashima, R., Yaono, R., Yamashita, E., Inoue, N., Yao, M., Fei, M. J., Libeu, C. P., Mizushima, T., Yamaguchi, H., Tomizaki, T., and Tsukihara, T. (1998) *Science* **280,** 1723–1729
7. Iwata, S., Ostermeier, C., Ludwig, B., and Michel, H. (1995) *Nature* **376,** 660–669
8. Klinman, J. P. (1996) *Chem. Rev.* **96,** 2541–2562
9. Smirnova, I. A., Zaslavsky, D., Fee, J. A., Gennis, R. B., and Brzezinski, P. (2008) *J. Bioenerg. Biomembr.* **40,** 281–287
10. Szundi, I., Funatogawa, C., Fee, J. A., Soulimane, T., and Einarsdóttir, O. (2010) *Proc. Natl. Acad. Sci. U.S.A.* **107,** 21010–21015
11. Kim, Y., Shinzawa-Itoh, K., Yoshikawa, S., and Kitagawa, T. (2001) *J. Am. Chem. Soc.* **123,** 757–758
12. Fern, W. O. (1932) *Am. J. Physiol.* **102,** 379–392
13. Young, L. J., and Caughey, W. S. (1986) *Biochemistry* **25,** 152–161
14. Proshlyakov, D. A., Pressler, M. A., and Babcock, G. T. (1998) *Proc. Natl. Acad. Sci. U.S.A.* **95,** 8020–8025
15. Michel, H. (1999) *Biochemistry* **38,** 15129–15140
16. Budiman, K., Kannt, A., Lyubenova, S., Richter, O. M., Ludwig, B., Michel, H., and MacMillan, F. (2004) *Biochemistry* **43,** 11709–11716
17. Wiertz, F. G., Richter, O. M., Cherepanov, A. V., MacMillan, F., Ludwig, B., and de Vries, S. (2004) *FEBS Lett.* **575,** 127–130
18. Hellwig, P., Pfitzner, U., Behr, J., Rost, B., Pesavento, R. P., Donk, W. V., Gennis, R. B., Michel, H., Ludwig, B., and Mäntele, W. (2002) *Biochemistry* **41,** 9116–9125
19. Tomson, F., Bailey, J. A., Gennis, R. B., Unkefer, C. J., Li, Z., Silks, L. A., Martinez, R. A., Donohoe, R. J., Dyer, R. B., and Woodruff, W. H. (2002) *Biochemistry* **41,** 14383–14390
20. Luna, V. M., Chen, Y., Fee, J. A., and Stout, C. D. (2008) *Biochemistry* **47,** 4657–4665
21. Koutsoupakis, C., Soulimane, T., and Varotsis, C. (2003) *J. Am. Chem. Soc.* **125,** 14728–14732
22. Koutsoupakis, C., Soulimane, T., and Varotsis, C. (2004) *Biophys. J.* **86,** 2438–2444
23. Stavrakis, S., Koutsoupakis, K., Pinakoulaki, E., Urbani, A., Saraste, M., and Varotsis, C. (2002) *J. Am. Chem. Soc.* **124,** 3814–3815
24. Pinakoulaki, E., Soulimane, T., and Varotsis, C. (2002) *J. Biol. Chem.* **277,** 32867–32874
25. Woodruff, W. H. (1993) *J. Bioenerg. Biomembr.* **25,** 177–188
26. Kannt, A., Lancaster, C. R., and Michel, H. (1998) *Biophys. J.* **74,** 708–721
27. McCauley, K. M., Vrtis, J. M., Dupont, J., and van der Donk, W. A. (2000) *J. Am. Chem. Soc.* **122,** 2403–2404
28. Aki, M., Ogura, T., Naruta, Y., Le, T. H., Sato, T., and Kitagawa, T. (2002) *J. Phys. Chem. A* **106,** 3436–3444
29. Cappuccio, J. A., Ayala, I., Elliott, G. I., Szundi, I., Lewis, J., Konopelski, J. P., Barry, B. A and Einarsdóttir, O. (2002) *J. Am. Chem. Soc.* **124,** 1750–1760
30. Daskalakis, V., Pinakoulaki, E., Stavrakis, S., and Varotsis, C. (2007) *J. Phys. Chem. B* **111,** 10502–10509
31. Morgan, J. E., Verkhovsky, M. I., Palmer, G., and Wikström, M. (2001) *Biochemistry* **40,** 6882–6892
32. Pinakoulaki, E., Pfitzner, U., Ludwig, B., and Varotsis, C. (2002) *J. Biol. Chem.* **277,** 13563–13568
33. Han, S., Ching, Y. C., and Rousseau, D. L. (1990) *J. Am. Chem. Soc.* **112,** 9445–9451
34. Pinakoulaki, E., Pfitzner, U., Ludwig, B., and Varotsis, C. (2003) *J. Biol. Chem.* **278,** 18761–18766
35. Varotsis, C., Woodruff, W. H., and Babcock, G. T. (1990) *J. Biol. Chem.* **265,** 11131–11136
36. Delano, W. L. (2010) *The PyMOL Molecular Graphics System*, Version 1.3, Schrödinger, LLC, New York
37. Chang, H. Y., Hemp, J., Chen, Y., Fee, J. A., and Gennis, R. B. (2009) *Proc. Natl. Acad. Sci. U.S.A.* **106,** 16169–16173